Journal of Catalysis **191,** 373–383 (2000)
doi:10.1006/jcat.1999.2795, available online at http://www.idealibrary.com on IDEAL®

Raman and X-Ray Absorption Studies of Mo Species in Mo/H-ZSM5 Catalysts for Non-Oxidative CH_4 Reactions

Wei Li, George D. Meitzner,* Richard W. Borry III, and Enrique Iglesia[1]

*Materials Sciences Division, E.O. Lawrence Berkeley National Laboratory, and Department of Chemical Engineering, University of California, Berkeley, California 94720; and *Edge Analytical, 2126 Allen Boulevard, Middleton, Wisconsin 53562*

Received September 7, 1999; revised December 10, 1999; accepted December 13, 1999

The structure of MoO_x and MoC_y species in Mo/H-ZSM5 after exchange and during CH_4 reactions was probed by *in situ* Raman and X-ray absorption spectroscopy. Raman spectra of physical mixtures of H-ZSM5 and MoO_3 powders initially showed strong Raman bands characteristic of bulk MoO_3. The intensity of Raman bands for Mo–O–Mo decreased relative to those for Mo=O bonds during treatment in air at 773 K, suggesting that MoO_3 spreads as $(MoO_3)_n$ oligomers on external zeolite surfaces. The Raman bands for MoO_3 crystallites became much weaker after treatment in air at 973 K; this occurred concurrently with H_2O evolution, indicating that dispersed MoO_x species exchanged with acidic OH groups in the zeolite. Weak bands appeared at 970 and 1045 cm^{-1}; they were assigned to stretching modes in exchanged MoO_x species. The X-ray near-edge spectrum of MoO_3/H-ZSM5 mixtures gradually evolves to one characteristic of tetrahedral Mo^{6+} centers in bulk $MgMo_2O_7$ as H_2O forms during treatment at 773–973 K, confirming that exchange occurs in this temperature range. Each Mo^{6+} replaces one H^+ at all Mo contents (Mo/Al = 0.11–0.37). The radial structure function derived from the absorption fine structure also evolves from that for bulk MoO_3, to that expected of dispersed MoO_3 without long-range periodicity, to one described using multiple scattering simulations as a $(Mo_2O_7)^{2-}$ dimer resembling $MgMo_2O_7$ with two of the O atoms located in the zeolite framework. This structure is consistent with the exchange stoichiometry from H_2O desorption and with the removal of 2.5 O/Mo during reduction-carburization. The required number of Al pairs in the samples to accommodate the dimer structures is within the range predicted by Monte Carlo calculation of Al statistical distribution. The absorption edge and near-edge features in exchanged MoO_x/H-ZSM5 evolve during CH_4 reactions at 973 K to resemble bulk Mo_2C without long-range periodicity, with the concurrent evolution of CO, CO_2, and H_2O and an increase in the rate of hydrocarbon formation. Multiple scattering analysis of a MoC_x cluster bonded to an O atom leads to a radial structure function in excellent agreement with experiment.

1. INTRODUCTION

In a previous study (1), we described indirect evidence for the formation of dispersed MoO_x species via solid-state exchange from physical mixtures of MoO_3 and H-ZSM5 powders. The resulting materials led to CH_4 conversion rates and selectivities similar to those reported for samples prepared by aqueous impregnation-exchange with ammonium heptamolybdate and treatment in air at 723–973 K (2–5). H_2O evolution rates during solid-state exchange at 973 K suggested that MoO_x species migrate on ZSM5 surfaces and ultimately replace one zeolitic H^+ per Mo to form $(Mo_2O_5)^{+2}$ dimers bridging two cation-exchange sites. In this study, we present *in situ* Raman and X-ray absorption spectroscopic evidence for the structure of MoO_x species as they evolve during synthesis. We also describe the evolution of the active MoC_x species formed by reduction-carburization of these Mo dimers during CH_4 reactions.

Raman spectroscopy is a useful probe of the structure of bulk and dispersed MoO_x because it detects vibrational modes for bulk and supported species without requiring long-range order (6). As a result, it has been used in studies of dispersed Mo oxides on Al_2O_3, SiO_2, and ZrO_2 (7, 8); specifically, it was used to study the spreading of MoO_3 on Al_2O_3 and TiO_2 (9) because of the large Raman cross section of MoO_3 crystallites. Raman spectroscopy provides information about the domain size of dispersed MoO_x because large size polymolybdate species, but not monomolybdate species, show Raman bands at 200–250 cm^{-1}, corresponding to bridging Mo–O–Mo bending modes. The frequency of Mo=O terminal stretching modes in MoO_x species has been related to the strength of the Mo=O bonds [10]; the local coordination of Mo in MoO_x species, however, is difficult to determine from Raman spectra because of the significant overlap between Mo=O stretching frequencies for tetrahedral and octahedral Mo centers. Consequently, complementary methods are required in order to confirm the local coordination of MoO_x species.

[1] To whom correspondence should be addressed. E-mail: iglesia@cchem.berkeley.edu.

0021-9517/00 $35.00

X-ray absorption spectroscopy (XAS) probes the local structure of an absorber atom within complex solids (11). X-ray absorption spectra can be divided into two regions, defined in terms of the energy range and of the information that each region provides. The absorption edge position and the spectral features near the edge (XANES) depend on the oxidation state and coordination symmetry of the absorber. The extended X-ray absorption fine structure (EXAFS) arises from scattering of ejected photoelectrons by neighboring atoms and reflects the local structure around the absorber (12). XANES can distinguish octahedral and tetrahedral Mo^{6+} centers in MoO_x species dispersed on Al_2O_3 (13) and several studies have reported X-ray absorption spectra of bulk Mo compounds with known structure (14, 15). The position of the X-ray absorption K-edge has been used to determine the Mo oxidation state in many bulk compounds (16).

This study addresses the structure of MoO_x and MoC_y species in Mo-exchanged H-ZSM5 samples using *in situ* Raman and X-ray absorption spectroscopy. In contrast to the extensive studies on MoO_x species on alumina, silica, and titania, only one study has used Raman spectroscopy to characterize MoO_x dispersed in zeolites (17), because the typical strong fluorescence from adsorbed species in zeolites prevents the detection of Raman bands. The pretreatment procedure described here minimizes fluorescence and leads to cleaner Raman spectra by removing adsorbed hydrocarbons. These Raman spectra clearly detect the migration and the structure of MoO_x species during synthesis of Mo/H-ZSM5 via solid-state exchange. The evolution of Mo species during solid-state exchange and during catalytic CH_4 reactions requires that spectroscopic methods be used as these transformations occur in order to determine the structure of the dispersed MoO_x precursor and the carburized MoC_y species which are active for methane conversion. Both Raman and X-ray absorption spectroscopies are well suited for the required *in situ* studies.

2. EXPERIMENTAL

2.1. Synthesis of MoO_x/H-ZSM5 Samples

Mo/H-ZSM5 samples were prepared from mixtures of MoO_3 (Johnson Matthey, 99.5% purity) and H-ZSM5 (Zeochem, Si : Al = 14.3) powders by mixing with a mortar and pestle and treating these mixtures in flowing dry air using temperature-programmed methods (10 K/min), with isothermal holds at 623 K (6 h), 773 K (6 h), and 973 K (0.5 h). The details of the synthesis and of several characterization methods have been reported elsewhere (1). The initial mixtures contained 1.1, 2.2, and 4.0% wt Mo, corresponding to Mo/Al ratios of 0.11, 0.22, and 0.42 respectively, and they are denoted as Mo-1, Mo-2, and Mo-4, respectively, throughout this paper. After thermal treatment in dry air at 973 K, the exchanged Mo-1, Mo-2, and Mo-4 samples contained 1.0, 2.0, and 3.6% wt Mo, corresponding to Mo/Al ratios of 0.11, 0.20, and 0.37, respectively. Dealumination occurred during treatment at 973 K, resulting in a Si/Al_F ratio of ~19 (from NMR and residual OH group measurements (1)); the Mo/Al_F ratios (Al_F: framework Al) in the exchanged samples are 0.14, 0.26, and 0.48 for Mo-1, Mo-2, and Mo-4, respectively.

2.2. Raman Spectroscopy

Raman spectra were measured before and after *ex situ* thermal treatments in flowing dry air at 973 K, and during *in situ* treatments in flowing 20% O_2/He at temperatures up to 873 K. Thin sample wafers (10 mm diameter) were prepared by pressing powders at 69 MPa in a uniaxial press (Carver, Inc.). The wafers were treated in flowing dry air while the temperature was increased at 10 K/min with isothermal soaks at 623 K (3 h), 773 K (3 h), and 973 K (9 h). The wafers were then removed from the heated furnace and placed quickly into a controlled atmosphere Raman cell before cooling to room temperature. Finally the samples were treated in flowing 20% O_2/He (100 cm^3/min) at 773–873 K before measurement of their spectra at room temperature.

The Raman spectra were measured using a HoloLab 5000 Research Raman Spectrometer (Kaiser Optical Systems, Inc.) equipped with a 532-nm diode-pumped solid-state laser (Coherent Laser Group). A CCD camera thermoelectrically cooled to 233 K was used as the detector (Princeton Instruments, Inc.). The *in situ* Raman cell has been described previously (18). The laser power at the sample was 75 mW, the spectral resolution was 5 cm^{-1}, and the wafers were rotated at ~500 rpm in order to minimize laser heating.

2.3. Mo K-Edge X-Ray Absorption Spectroscopy

X-ray absorption spectra were measured using beamlines 4-1 and 4-3 at the Stanford Synchrotron Radiation Laboratory (SSRL). Spectra were measured in transmission mode with Ar in three individual ion chamber detectors: one before the sample to measure the incident X-ray intensity I_0, one after the sample and before a Mo foil (7.5 μm) to measure the intensity after the sample I_1, and one after the Mo foil in order to measure the intensity after the Mo foil I_2. The sample spectrum and the Mo foil spectrum were expressed as $\log(I_0/I_1)$ and $\log(I_1/I_2)$, respectively. The spectrum from the Mo foil was used to calibrate the absolute energy scale for a corresponding sample spectrum, by positioning the first inflection point in the Mo edge at 19.999 keV. Monochromators on both beamlines were equipped with Si(220) crystals, detuned to 50% of the maximum inlet X-ray intensity in order to minimize harmonics. The 0.2-mm vertical aperture of the beam definition slit in the hutch provided a resolution of about 2.5 eV at the Mo K absorption edge (19.999 keV) (19). Spectra were measured with an increment of 5 eV in the pre-edge region

from 19.875 to 19.975 keV, 0.25 eV in the edge region between 19.975 and 20.025 keV, and 0.04 $Å^{-1}$ from 20.025 to 21.024 keV.

$MgMo_2O_7$ (prepared by the procedure in Ref. (20)), $Al_2(MoO_4)_3$ (GFS Chemicals, 99%), $(NH_4)_2Mo_2O_7$ (Strem Chemicals, 99.98%), and Mo_2C (prepared as in Ref. (21)) were diluted with SiO_2 to 4 ± 0.5 wt% Mo, pressed into wafers, and sealed in Kapton tape (3M Co.). These samples were used as standards in the structural analysis of MoO_x/H-ZSM5 samples. The bulk Mo_2C standard was exposed to ambient air during dilution and pressing; thus, it was partially oxidized. MoO_3/H-ZSM5 powder mixtures and previously exchanged MoO_x/H-ZSM5 samples were pressed into wafers, crushed, and sieved to retain particles with 0.18- to 0.25-mm diameter. These particles were placed within thin quartz capillaries (1.0-mm diameter; 0.1-mm wall thickness) and supported horizontally in the path of the rectangular X-ray beam (0.2×6.0 mm). Four heat cartridges within a copper block were used to heat the capillary cell (22). Samples were dehydrated by treating them in dry air (2 cm^3/min, Matheson, Ultra Zero) at 973 K for 2 h. Air and other gases (He, CH_4/Ar, and H_2; Matheson, chemical purity >99.995%) were introduced using a portable gas manifold that included electronic mass flow controllers (Porter Instrument Co.) and purification traps for the removal of water and hydrocarbons.

X-ray absorption data were analyzed using WinXAS (version 1.2) (23). A linear fit to the pre-edge region was subtracted from the entire spectrum, and then the spectrum was normalized using a fifth-order polynomial fit to the post-edge (EXAFS) region. The XANES region of the spectra was analyzed between 19.908 and 20.158 keV. The energy scale for conversion to k (wave vector)-space was calibrated by defining the first inflection point, or the first inflection point beyond the pre-edge peak (if present), as 0 eV. After conversion to k-space, the EXAFS weighted by k^1 was Fourier-transformed between 2.2 and 15.9 $Å^{-1}$. Fourier-transformed EXAFS was fit between 0.5 and 8 Å with inputs calculated by FEFF 6.0 (24). The FEFF simulation to a radius of 4 Å led to 6 single-scattering and 20 multiple-scattering shells with individual amplitudes greater than 5% of the amplitude of the strongest shell. This simulation was refined in real space by varying one amplitude reduction factor S_0^2, one E_0 shift for each atom type or a total of 3 E_0 shifts, and the 6 single-scattering distances. The multiple-scattering distances were constrained to accommodate the adjustments in the single-scattering distances, and Debye-Waller factors were set to zero.

3. RESULTS AND DISCUSSION

3.1. Raman Spectroscopy

Raman spectra of fresh MoO_3/H-ZSM5 mixtures show intense fluorescence during heating from 300 to 800 K in dry air. At these temperatures, hydrocarbons adsorbed from ambient air during grinding and pressing dehydrogenate to form unsaturated carbonaceous deposits that fluoresce in the spectral region of the incident laser light (25). Above 800 K, these deposits were gradually removed by combustion, but even after heating at 873 K (the maximum temperature of the cell), the remaining fluorescence was too strong to allow the detection of the weak Raman bands expected for dispersed MoO_x species in exchanged samples. This problem was encountered also in preexchanged powders, because samples adsorbed hydrocarbons during the preparation of the wafers. Treating the wafers *ex situ* in flowing dry air at 973 K for 9 h, and then placing them in the controlled atmosphere Raman cell before they cooled, minimized hydrocarbon adsorption and allowed detection of Raman bands for all Mo/Al ratios.

Before treatment in air, physical mixtures of MoO_3 and H-ZSM5 powders (Mo-4; Fig. 1a) showed Raman bands at 820 and 996 cm^{-1} and weaker bands around 300 cm^{-1}, corresponding to the antisymmetric stretching mode of Mo–O–Mo, the stretching mode of Mo=O, and the bending mode of Mo=O bonds in bulk MoO_3 crystallites, respectively (6). After treatment in flowing O_2/He at 773 K for 2 h, the intensity of the band at 820 cm^{-1} decreased relative to that at 996 cm^{-1} (Fig. 1b), indicating that the number of bridging Mo–O–Mo bonds decreases relative to the number of terminal Mo=O bonds. Also a weak shoulder started to appear at ~953 cm^{-1}, corresponding to polymeric molybdate species (6). These suggest that spreading of MoO_3 crystallites starts to occur on H-ZSM5 surfaces to form $(MoO_3)_n$ oligomers, but that the size of the oligomers remains large enough to show intense bands at 820 and 996 cm^{-1}. At 773 K the spreading of MoO_3 occurs, most

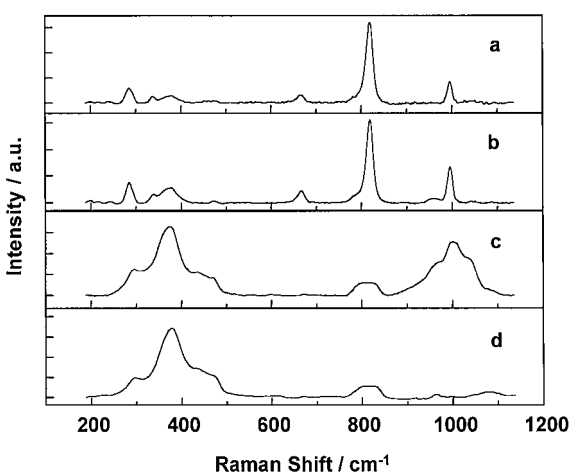

FIG. 1. Raman spectra of sample Mo-4 (a) starting physical mixture; (b) after *in situ* treatment in flowing 20% O_2/He at 773 K for 1 h; (c) treated in air at 973 K for 9 h, followed by *in situ* treatment in flowing 20% O_2/He at 773 K for 1 h. (d) Raman spectrum of H-ZSM5 after treatment in flowing 20% O_2/He at 973 K for 2 h.

likely on the external ZSM5 surface because the intensity of the infrared band corresponding to the Brønsted acid sites did not decrease (27), and H_2O desorption during exchange was only observed at >773 K (1). *Ex situ* treatment of the sample wafers in dry air at 973 K for 9 h led to significant changes in the spectrum (Fig. 1c). The bands at 820 and 996 cm^{-1} became much weaker, indicating that MoO_3 crystallites dispersed during treatment in air at 973 K. Weak bands corresponding to framework vibrations in H-ZSM5 (28, 29) appeared at 376 and 820 cm^{-1} after these treatments (Fig. 1d). The overlap of the zeolite band at 820 cm^{-1} with the strongest band in crystalline MoO_3 prevented us from excluding the presence of residual traces of crystalline MoO_3. The Raman cross section of bulk MoO_3, however, suggests that the residual concentration of MoO_3 crystallites must be very small. New bands appeared after this treatment at 970, 1000, and 1045 cm^{-1}, and their assignment is discussed below.

Figure 2 compares Raman spectra of exchanged MoO_x/H-ZSM5 samples with different Mo content after *ex situ* treatments in flowing dry air at 973 K for 9 h. Because of the absence of the strong bands corresponding to MoO_3 crystallites, the lattice vibrations for H-ZSM5 were detected at 376 and 820 cm^{-1} in all samples, indicating that the crystalline zeolite framework was preserved during exchange, in agreement with previous porosimetry and X-ray diffraction data (1). The spectra showed bands at 970, 1000, and 1045 cm^{-1} for all samples, indicating that similar MoO_x species exist in all of them. As the Mo content increased, the intensity ratio of the band at 970 cm^{-1} to that at 1045 cm^{-1} remained almost constant, but the ratio of the 1000 cm^{-1} band intensity to the intensities of the 970 and 1045 cm^{-1} bands increased. This suggests that the bands at 970 and 1045 cm^{-1} arise from the same MoO_x species, that the band at 1000 cm^{-1} corresponds to a different type of MoO_x species, and that the density of the species related to the 1000 cm^{-1} band increases with increasing Mo content.

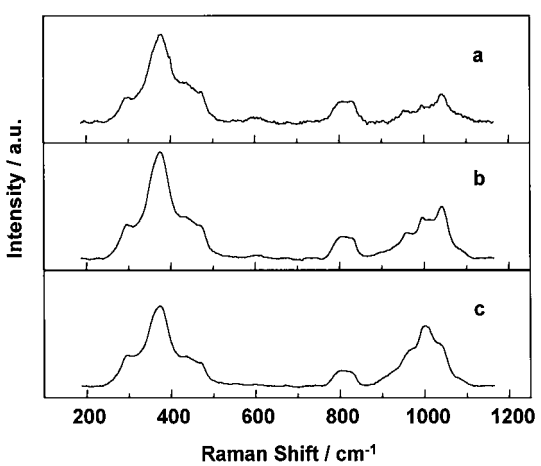

FIG. 2. Raman spectra of samples Mo-1 (a), Mo-2 (b), and Mo-4 (c) after treated in air at 973 K. For Mo-1 and Mo-2 samples, spectra were acquired after *in situ* treatment at 873 K for 1 h in 20% O_2/He flow. For Mo-4, the *in situ* treatment was carried out at 773 K.

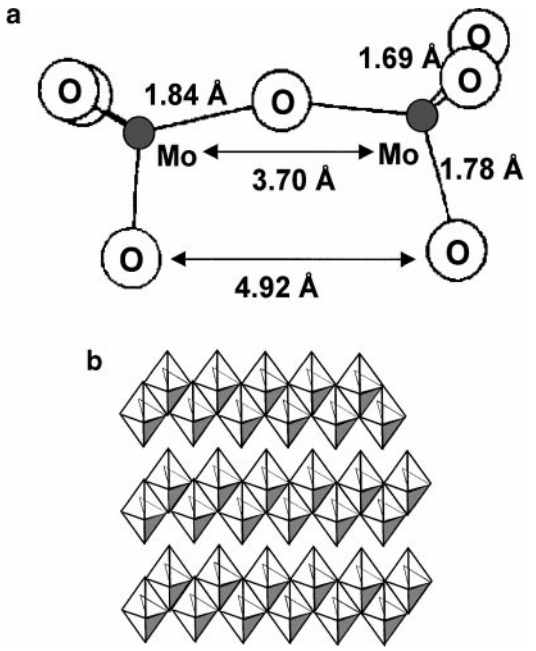

FIG. 3. (a) The ditetrahedral structure in $MgMo_2O_7$ and (b) the bilayer structure of bulk MoO_3. The bond lengths shown in (a) were obtained from refinement of FEFF simulation for the EXAFS of MoO_x species in the exchanged sample.

The band detected at 1000 cm^{-1} has been assigned to Mo=O stretching modes in isolated monomolybdate species (30). Therefore, we assign it to the stretching mode of M=O bonds in isolated species on the external surface of ZSM5. The band at 1045 cm^{-1} has not been reported previously. We attribute this band and that at 970 cm^{-1} to the stretching modes of Mo=O bonds in exchanged MoO_x species within ZSM5 channels. This assignment is consistent with a $(Mo_2O_5)^{2+}$ dimer structure (Fig. 3a) in which each Mo is bonded to a framework oxygen. The formation of these species was recently inferred from measurements of the H_2O desorption during exchange and of the remaining Brønsted acid sites using D_2–OH exchange in these samples (1). A symmetry analysis for species X_2O_7 of C_{2v} symmetry (31) predicts two terminal stretching modes of *A1* symmetry. Vibrational modes with *A1* symmetry usually give the strongest Raman bands. The band at 1000 cm^{-1} of isolated Mo species is of *A1* symmetry and thus visible even at very low concentrations of these species. Therefore, the presence of two Raman bands in the Mo=O stretching regions (Fig. 2) is consistent with the $(Mo_2O_5)^{2+}$ dimer structure and the new bands at 1045 and 970 cm^{-1} can be assigned to the two terminal stretching modes of $(Mo_2O_7)^{2-}$. The band at 1045 cm^{-1} has a higher frequency than monomolybdate bands of MoO_x/SiO_2 samples (1000 cm^{-1}); this suggests either that MoO_x species in exchanged samples have shorter Mo=O bonds than the monomolybdate species in

MoO_x/SiO_2 samples or that their structures are distorted by the restricted environment within ZSM5 channels (32). For the sample with the lowest Mo content (Mo-1), the most intense band appeared 1045 cm^{-1}, but the band at 1000 cm^{-1}, corresponding to unconstrained monomolybdate species, became more intense as the Mo content increased, suggesting that the concentration of residual isolated MoO_x species on ZSM5 external surfaces increased with increasing Mo content.

The proposed structure of $(Mo_2O_5)^{2+}$ requires that framework oxygens connected to Al atoms reside within 4.2–5.5 nm of each other. Assuming random Al occupancy at T sites, the fraction of the Al atoms residing within the distance of another Al for a Si/Al_F ratio of 19 (estimated value after treatment at 973 K) is about 0.34 (12). Therefore, samples with Mo/Al_F ratios of 0.14 and 0.26 (Mo-1, Mo-2) contain enough Al pairs to accommodate all Mo species as dimers. The sample with a Mo/Al_F ratio of 0.48 (Mo-4), however, requires the migration of Al atoms during treatment in order to accommodate the larger number of Mo dimers. The required mobility is likely to be achieved at the high temperatures required for exchange, evidenced by the detected dealumination. Migration stops when Al sites containing $(MoO_2OH)^+$ monomers approach another monomer and desorption of water occurs by condensation reactions leading to a bridging in a Mo dimer (Eq. [1]). The resulting Mo dimers stabilize the structure against further dealumination; they appear to provide a thermodynamic endpoint that becomes kinetically accessible at the high temperatures of the exchange process. The thermodynamic stability of this species leads to identical structures, although the Mo content and the synthesis methods change.

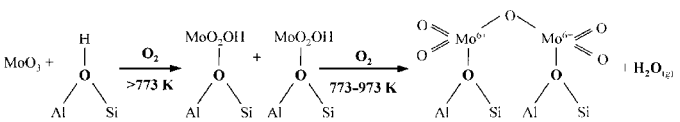

[1]

The disappearance of X-ray diffraction lines of MoO_3 during treatment in air below 773 K was reported in earlier studies on MoO_x/H-ZSM5 and was attributed to the dispersion of MoO_3 onto external zeolite surfaces (1, 33). Raman spectra of MoO_3/H-ZSM5 mixtures treated at 773 K (Fig. 1), however, showed intense bands of crystalline MoO_3 at 820 and 996 cm^{-1}. The apparent discrepancy arises from the different domain sizes required for detection of crystallinity in the two methods. X-ray diffraction detects crystallites with diameters larger than ~2 nm, while Raman detects vibrational modes of much smaller MoO_3 clusters, as previously discussed for MoO_3 dispersed on Al_2O_3 (34).

3.2. Mo K-Edge X-Ray Absorption Near-Edge Spectroscopy (XANES)

In situ Mo K near-edge spectra were measured for mixtures of MoO_3 and H-ZSM5 powders (Mo-4) during heating in flowing dry air (2 cm^3/min) at 10 K/min with isothermal holds at 623 K (6 h), 773 K (4 h), and 973 K (2 h). Several spectra (3–10) were measured at each temperature; these spectra were averaged in order to improve the quality of the spectra. Spectra measured at 973 K remained unchanged after cooling to 300 K, showing that thermal vibrations do not influence the spectra measured at high temperatures. The Mo K edge was observed at ~20 keV, reflecting the ejection of a Mo 1*s* photoelectron (Fig. 4). For comparison, the near-edge spectra for Mo metal, Mo_2C, MoO_3, and $MgMo_2O_7$ are shown in Fig. 5. The pre-edge feature at ~19.99 keV reflects a 1*s* to 4*d* electronic transition that is dipole-forbidden in centrosymmetric octahedral structures. Mo^{6+} cations in MoO_3 occupy off-center positions in distorted MoO_6 octahedra (Fig. 3b) and this distortion allows the dipole-forbidden transition to occur. Recently, it has also been argued that the coordination of Mo in MoO_3

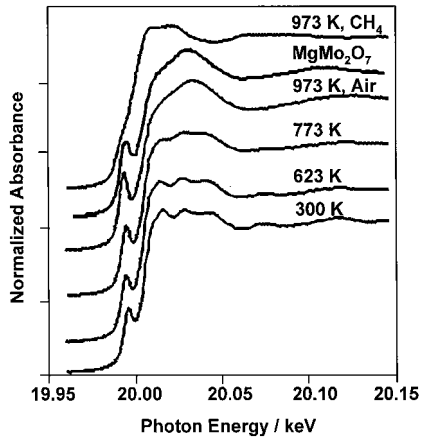

FIG. 4. Mo K-edge X-ray absorption spectra of sample Mo-4 during treatments in air or CH_4 (2 cm^3/min). The spectrum of $MgMo_2O_7$ is also shown for comparison.

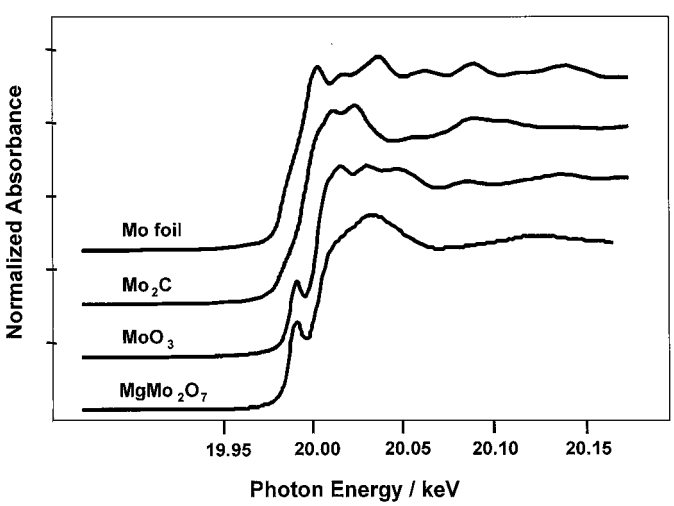

FIG. 5. Mo K-edge X-ray absorption spectra of Mo standard compounds (near edge region).

is fourfold and the lattice of MoO_3 is better described by chains of tetrahedral MoO_4 units (6). In either case, the deviation from perfect octahedral symmetry of the Mo centers in MoO_3 results in the appearance of the pre-edge feature in its XANES. The intensity of this pre-edge feature increases with increasing tetrahedral symmetry of the Mo^{6+} centers because of increasing *p–d* orbital mixing (35).

The near-edge spectra of the initial MoO_3/H-ZSM5 physical mixtures (Fig. 4) resembled that for bulk MoO_3. The near-edge spectra did not change as these mixtures were treated in air at temperatures between 300 and 623 K, indicating that the local structure around Mo centers was not affected by this treatment. MoO_x may migrate at these temperatures, while preserving the bonds within layers and without detectable changes in local symmetry. At 773 K, the near-edge spectra changed slightly (Fig. 4), suggesting that incipient structural transformations changed the local environment around Mo atoms. The absorption edge energy and the near-edge spectral features, however, remained similar to those for distorted MoO_6 octahedra in bulk MoO_3. The near-edge features remained unchanged, because the dispersion of MoO_3 as a layer structure occurs via an "unrolling-carpet" mechanism, which preserves the bonding within MoO_3 layers in crystalline MoO_3 almost intact but which delaminates the structure by breaking weak van der Waals bonding between layers (9).

Between 773 and 973 K, near-edge spectra began to resemble those measured for tetrahedral Mo^{6+} species in $MgMo_2O_7$ (Fig. 4). A principal component analysis (PCA) of the spectra taken for the Mo-4 sample during heating at 1 K min^{-1} in air from 293 to 973 K, detected contributions to the spectra from two major Mo^{6+} species. These were identified as the residual MoO_3 crystallites from the starting material and as a structure similar to dimolybdate anions in $MgMo_2O_7$. Figure 6 shows a representative fit for contributions from MoO_3 and $MgMo_2O_7$ near-edge spectra of 70 and 30%, respectively, to the near-edge spectrum of Mo-4 in air at 860 K. Figure 7 shows the relative amounts of MoO_3 and $MgMo_2O_7$ obtained from these spectra as a function of temperature; the dotted curve represents the rate of water evolution measured by mass spectrometry of the effluent stream. The observed changes in local Mo symmetry coincide with the evolution of water during exchange, a process previously attributed to the anchoring of $(Mo_2O_5)^{2+}$ dimers at cation-exchange sites with the replacement of 2 H^+ (1). These data show that exchange of MoO_x species at cation-exchange sites occurs simultaneously with the changes in local symmetry detected by X-ray absorption. $Al_2(MoO_4)_3$ species, which also lead to structural changes and to water evolution, would not lead to the observed exchange stoichiometry and they were not detected by ^{27}Al NMR or Raman spectroscopy in this sample (1). Thus, it does not appear that the tetrahedral Mo species detected by XAS correspond to the formation of $Al_2(MoO_4)_3$. No new ^{27}Al NMR signal was detected for Al

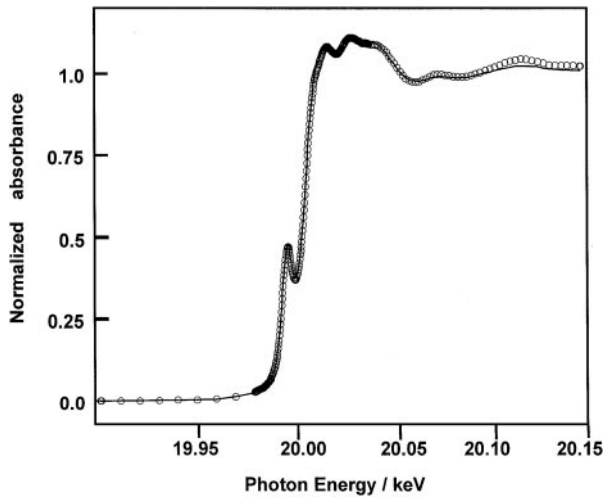

FIG. 6. A representative fit of the Mo K-edge X-ray absorption spectrum of sample Mo-4 during exchange. The solid line represents the measured spectrum and the symbol ○ represents the linear combination fit using 70% MoO_3 and 30% $MgMo_2O_7$.

bonded to the $(Mo_2O_7)^{2-}$ species in the exchanged samples, and the amount of detectable Al decreased with increasing Mo content. This may reflect the asymmetric nature of the ditetrahedral species, in which tetrahedral Al centers are bonded to tetrahedral Mo centers. We could not find an Al–Mo–O compound with this coordination symmetry. For example, $Al_2(MoO_4)_3$ has octahedral Al centers bonded to tetrahedral Mo, while Al_2O_3-supported MoO_x catalysts contain either octahedral or tetrahedral Mo bonded to octahedral Al centers. This suggests that the structure of

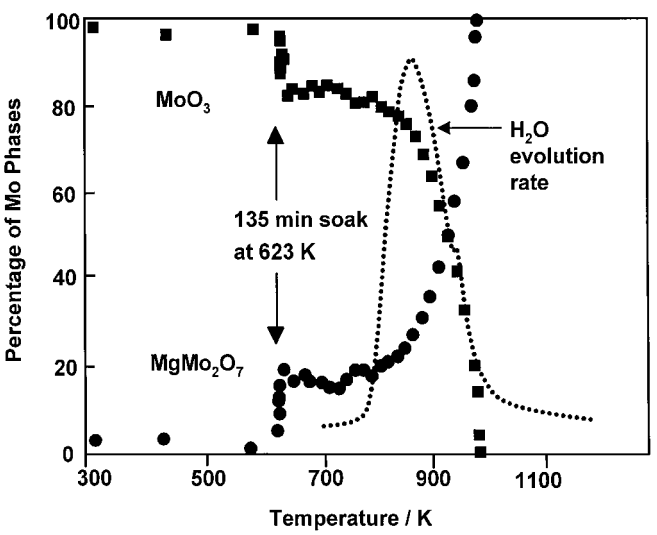

FIG. 7. PCA analysis results of the Mo K-edge X-ray absorption spectra of sample Mo-4 after treatment at various temperatures. Also shown in the figure is a plot of water evolved (dotted line) during the exchange measured by mass spectrometry.

TABLE 1

Edge Energy Positions of Mo (Relative to Mo Foil, E_0) in Standard Compounds and in Mo/H-ZSM5 Catalysts

Sample	Absorption edge energy $(E - E_0)$/eV
Mo foil	0
Mo_2C	1.0
MoO_3	6.6
$(NH_4)_2Mo_2O_7$	4.2
$(NH_4)_2Mo_7O_{24}$	4.5
Mo-4[a]	5.1
Carburized Mo-4[b]	0.9

Note. The energy position of the absorption edge was defined as the first inflection point, or the first inflection point beyond the preedge peak (if present).

[a] The sample was treated at 973 K in dry air for 2 h.

[b] The sample was carburized at 973 K in CH_4 for 1 h.

the $(Mo_2O_7)^{2-}$ anions is strained, as expected from the range of distances and orientations in the (Al---Al) site pairs required to anchor it and from the confined environment within the zeolite channels.

After treatment in air for 2 h at 973 K, Mo/H-ZSM5 samples were cooled in He (2 cm^3/min) to room temperature and several spectra were measured. The samples were then heated to 973 K in He, and the flowing gas was switched to a CH_4/Ar reactant mixture (1 : 1, 2 cm^3/min). The Mo–K edge spectrum started to change immediately, and it reached a stable spectrum within about 0.5 h (Fig. 4). The absorption edge energies in samples before and after heating in air, and after carburization in CH_4, are shown in Table 1. The absorption edge energy for carburized Mo/H-ZSM5 samples corresponds to 0.9 eV above the edge energy in Mo foil; it is in good agreement with the edge energy measured for Mo_2C, indicating that Mo^{6+} centers in $(Mo_2O_5)^{2+}$ reduce and carburize to form MoC_y. A fit of the edge spectra during carburization was carried out using linear combinations of the edge spectra of the starting exchanged sample and of the final carburized sample (Fig. 8). The changes in the edge spectrum coincided with oxygen removal (rate shown as dashed line in Fig. 8), detected by mass spectrometry from the evolution of CO, CO_2, H_2O, and H_2 during the initial contact with CH_4 (36, 37). CH_4 conversion to hydrocarbons increased as oxygen was removed and MoC_y species were formed (Fig. 9), suggesting that carburized species provide catalytic active centers for hydrocarbon formation from methane. $(Mo_2O_5)^{2+}$ dimers formed during exchange are not active in the formation of hydrocarbons but they activate C–H bonds in methane to form CO_x, H_2O, and H_2 with the concurrent reduction of Mo^{6+} centers. Reduction-carburization processes remove 2.5 O atoms per Mo; thus all the oxygens in the $(Mo_2O_5)^{2+}$ dimer structure, but none of the framework oxygens, are removed. Benzene formation rates reached a maximum when the $O_{removed}$/Mo ratio was about 1.7, and decreased with further reaction, because coke deposition leads to concurrent catalyst deactivation and activation processes (36).

Principal component analysis of the near-edge spectra in carburized samples was not conclusive. It showed that three Mo species contribute to the evolution of the spectra during exposure to CH_4. One spectral component is the ditetrahedral Mo species in the exchanged sample, but the other two could not be assigned to known Mo compounds. MoO_3 and Mo_2C were specifically rejected as significant components of the spectra. A MoO_3 component is not likely, because exchange appears to eliminate all contributions from bulk MoO_3 to exchanged samples. Bulk Mo_2C was also rejected as a significant component in carburized samples. It is likely that the MoC_y species formed from the oxide dimers are highly dispersed, probably as monomers; therefore they lack the long-range order required for the multiple-scattering features that contribute to the near-edge spectra features in large Mo_2C crystallites. The structure of these MoC_y species is suggested in the next section on the basis of evolution of the radial structure function during the initial stages of CH_4 reactions.

3.3. Extended X-Ray Absorption Fine Structure

Figure 10 shows the radial structure function of standard Mo compounds: Mo foil, Mo_2C, $MgMo_2O_7$, and MoO_3. The extended fine structure in the X-ray absorption spectra (~1000 eV above the edge) reflects the scattering of ejected electrons by atoms near the absorbing Mo centers (11). The radial structure functions obtained by Fourier transform of post-edge absorption data give distances between neighboring electron clouds; as a result, they are smaller than the actual interatomic distances between nuclei.

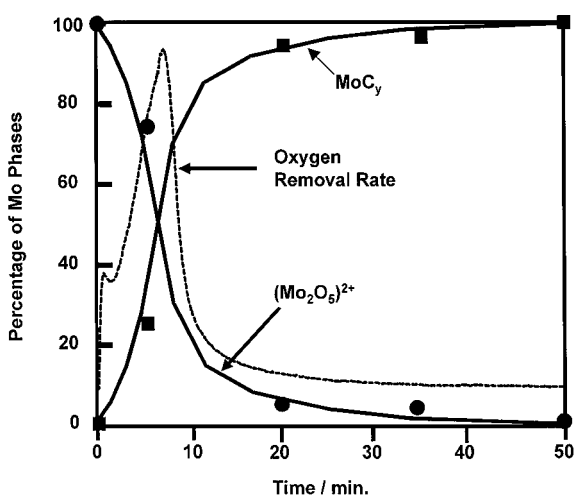

FIG. 8. PCA analysis results of the Mo K-edge X-ray absorption spectra of sample Mo-4 during carburization at 973 K in CH_4. Also shown in the figure is a plot of oxygen removal rate (dashed line) during the carburization reaction measured by mass spectrometry.

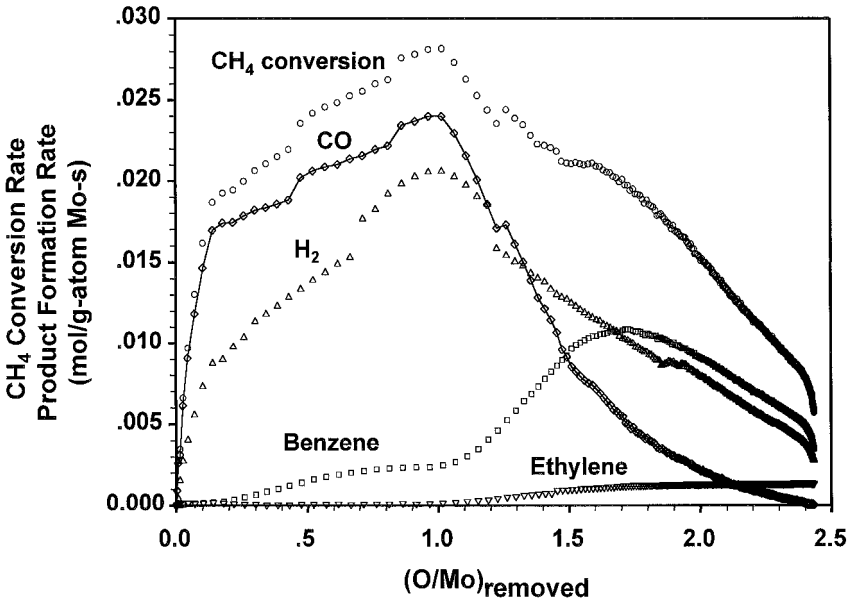

FIG. 9. CH_4 conversion and product (H_2, CO, C_6H_6, C_2H_4) formation rates as a function of the amount of oxygen removed during initial reduction-carburization period on Mo-4 (0.5 g, 950 K, 100 cm^3 min^{-1}, 1/1 CH_4/Ar).

MoO_3/H-ZSM5 physical mixtures showed multiple neighbor shells after treatment in air between 300 and 623 K (Fig. 11); these shells correspond to O nearest neighbors and Mo next-nearest neighbors in the bulk MoO_3 structure. At 773 K, the distance of the first Mo–O shell decreased slightly and the intensity of features beyond 3 Å decreased, as expected if large MoO_3 crystallites dispersed as $(MoO_x)_n$ oligomers. As octahedral Mo centers convert to tetrahedral structures during exchange at 973 K, the radial structure function shows only one peak at ~1.2 Å with a shoulder at about 0.8 Å. This radial structure function is nearly identical to that of isolated $(Mo_2O_7)^{2-}$ ditetrahedra in $MgMo_2O_7$ (Fig. 10). Such a structure is consistent with $(Mo_2O_5)^{2+}$ cations bonded via the Mo centers to two framework oxygens located at Al sites in the ZSM5 framework (Fig. 3a).

The fine structure from exchanged Mo-4 samples was compared with simulated spectra from model clusters including multiple-scattering calculations by the FEFF analysis software (24). $Na_2Mo_2O_7$, in which half the Mo atoms

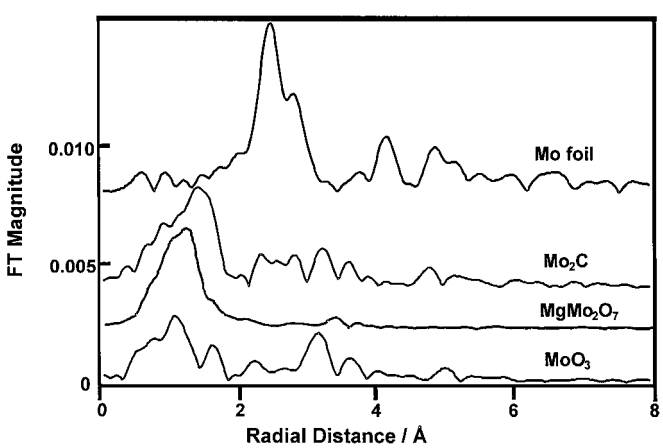

FIG. 10. Radial structure function of Mo in standard compounds: Mo foil, Mo_2C, $MgMo_2O_7$, and MoO_3. The radius represents distances between neighboring electron clouds, not nuclei.

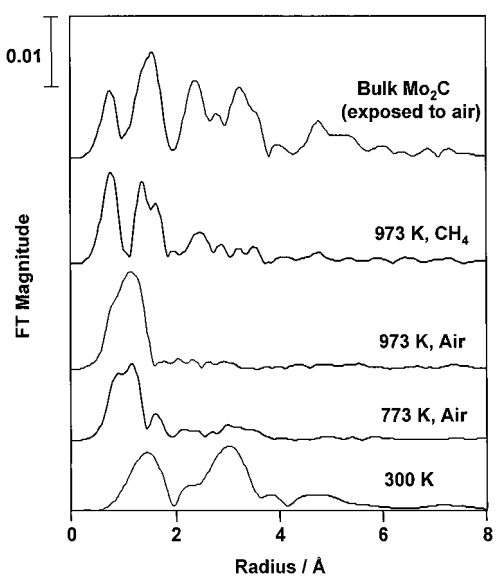

FIG. 11. Radial structure function generated from EXAFS of Mo-4 during *in situ* treatments in air or CH_4. The radius represents distances between neighboring electron clouds, not nuclei.

TABLE 2

Refined Structural Parameters for Dimolybdate Clusters in H-ZSM5

Shell	Coordination number	Interatomic distance (Å)	E_0 shift (eV)
Mo–O	1	1.69 ± 0.008	-4.64 ± 0.009
Mo–O	1	1.69 ± 0.008	-4.64
Mo–O	1	1.78 ± 0.0009	-4.64
Mo–O	1	1.84 ± 0.0009	-4.64
Mo–Mo	1	3.70 ± 0.0003	0.00 ± 0.01
Mo–Al	1	3.61 ± 0.0006	-10.09 ± 0.095

Note. Sample was treated in air at 973 K for 2 h. Coordination numbers for the structure shown in Fig. 5b were used in the simulation. Debye-Waller factors were fixed at zero. Only one value of energy shift was used for all four oxygen shells. The refined value of S_0^2 was 0.63.

are in octahedral sites (38), described poorly the experimental spectrum. The $MgMo_2O_7$ structure (20), in which both Mo atoms are tetrahedrally coordinated and connected via a bridging oxygen, provided a much better starting point when Al replaced the Mg atom. The fragment upon which the refinement was based is shown in Fig. 3a, and coordination numbers were all fixed at the values for the shown structure. The single-scattering parameters are shown in Table 2. Figure 12a shows the fit to the experimental radial structure function. Surprisingly, the third-shell Mo and Al neighbors, about 3.4 Å from a Mo atom, did not appear in the radial structure function. The reason for this is illustrated in Fig. 12b, for which the number of Mo neighbors was reset from 1 to 0, and all other parameters were kept fixed. In this case, the Al neighbor is clearly represented by a peak. In fact, the phase shifts imparted on the scattered photoelectron by interaction with Mo and Al neighbors at the same distance differ by π radians and the respective signals interfere destructively. In view of this, the absence of a third shell rules out the presence of monomeric Mo species proposed previously (39), for which this destructive interference would not occur; it supports instead the proposed $(Mo_2O_5)^{2+}$ dimer structure of Fig. 3a. The same model cluster was able to describe the structure of MoO_x species in a Mo/H-ZSM5 sample with lower Mo content (Mo/Al = 0.20) (27), suggesting that similar MoO_x species exist in Mo/H-ZSM5 samples with a wide range in Mo content (Mo/Al = 0.11–0.37). These results confirm our previous proposal (1) that MoO_x species in Mo/H-ZSM5 samples exist as $(Mo_2O_5)^{2+}$ dimers within ZSM5 channels. Their location as dispersed MoO_x within channels was also proposed by recent XAS studies (5, 40), without detailed analysis of the structure of such species or of their actual location at exchange sites.

When MoO_x/H-ZSM5 samples were exposed to CH_4 at 973 K, CO, CO_2, and H_2O formed as MoO_x species reduced and carburized to form MoC_y species (Eq. [2]), which provide active sites for CH_4 conversion to hydrocarbons (4, 29, 30). Evidence for the structure of these species was obtained by cluster simulations using multiple-scattering analysis methods and comparisons with radial structure functions obtained after exposure to CH_4 at 973 K for ~1 h (Fig. 13). The strong peaks near 1 and 2 Å are described by one oxygen neighbor at 1.7 Å and three carbon neighbors near 2.1 Å. Neither of the peaks, however, can be described using only oxygen or only carbon neighbors. The carbons may also retain bonded H atoms, which would not be detectable in the radial structure function. A description of the experimental data was initially attempted using three carbon shells at different distances, but only one Mo–C distance was required in order to describe the data. The Mo–C distance of 2.09 Å is within the range of bond lengths previously reported for Mo–C bonds in carbides (41). The Mo–Al distance of 3.66 Å is close to the Mo–Al distance of 3.61 Å in the Mo species formed after treatment in air at 973 K.

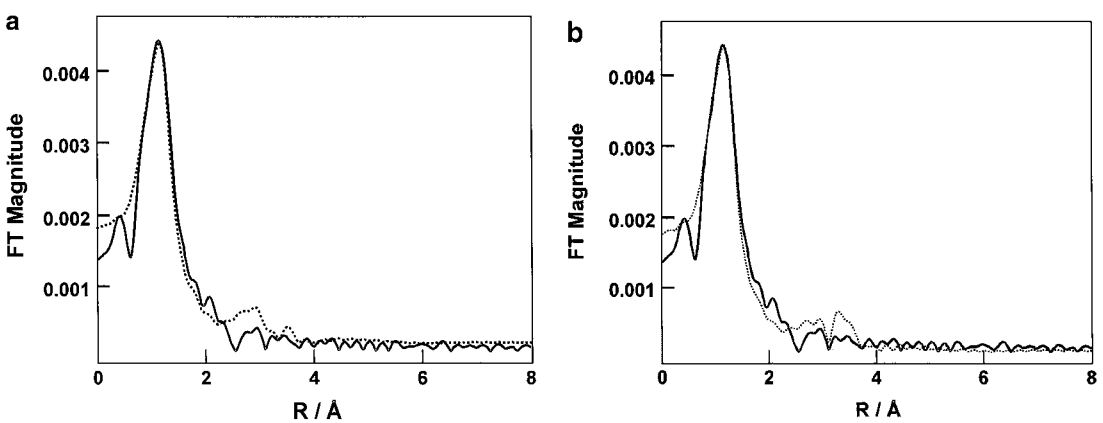

FIG. 12. (a) FEFF fit (dotted line) to Fourier-transformed EXAFS from Mo in exchanged Mo sample using the model structure shown in Fig. 3a. (b) FEFF fit (dotted line) to Fourier-transformed EXAFS from Mo in exchanged Mo sample using the same model structure except that the number of Mo neighbors is set to zero. The simulation parameters used are shown in Table 2.

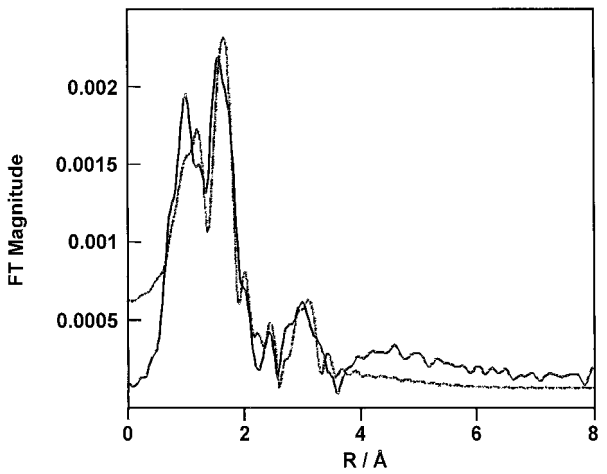

FIG. 13. FEFF fit (dotted line) to Fourier-transformed EXAFS from Mo in the carburized Mo-4 sample using the parameters shown in Table 3.

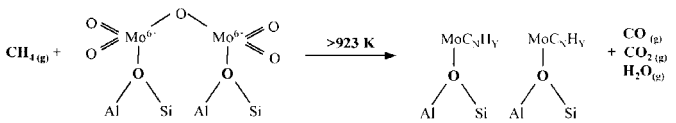

[2]

The radial structure functions of carburized sample show a small number of Mo–Mo pairs at a distance of 2.8 Å and some long-range shells (up to 5 Å) (Fig. 13). These features match closely those in bulk Mo_2C. Raman spectroscopy shows that after 2 h at 973 K, traces of MoO_x remain as octahedral MoO_x oligomers probably on external ZSM5 surface (responsible for the band at 1000 cm^{-1}). These species would convert to Mo_2C clusters in CH_4 at 973 K (42), and show long-range shells in the radial structure function. Based on the relative heights of the first two shells (corresponding to exchanged MoC_y species) and the long-range shells (corresponding to external Mo_2C), the amount of external Mo species must be relatively small ($\ll$10%). This is in agreement with the results from Raman and X-ray diffraction characterization of the exchanged samples (1, 33). These external Mo_2C species represent only a minor component and as in the case of bulk Mo_2C (43), they are not likely to be active in their unprotected extrazeolitic environment.

Recent work (36, 40, 43, 44) has provided strong evidence that carburized Mo species are the active sites for methane aromatization reaction; the location of these active MoC_y species, however, remains controversial. Lunsford and coworkers proposed that Mo_2C on external zeolite surfaces provides the required active sites, based on infrared, X-ray photoelectron spectroscopy, and ion-scattering measurements (44). A recent X-ray absorption study (45) also suggested that Mo_2C crystallites form on external zeolite surfaces, possibly as a result of MoO_x species inside the ZSM5 channels migrating to the external surface and carburizing upon contact with CH_4. On the other hand, an X-ray absorption study by Zhang *et al.* (40) and our work (27) based on XAS and infrared measurements have shown that MoC_y resides predominately within zeolite channels. These apparently contradictory reports may reflect the varying level of exchange among the studies and the tendency of most spectroscopy methods to emphasize the larger and more accessible crystallites that form in incompletely exchanged samples. The extent of exchange can be influenced by the synthesis procedure, most importantly by the temperature protocols during treatment in air, and by the Mo/Al_F ratio. These affect the availability and the kinetic accessibility of exchange sites during synthesis. Despite these differences, there tends to be general agreement on the catalytic performance of these materials, perhaps not surprisingly in view of their high activity and of their frequent operation near methane conversion equilibrium.

The radial structure functions for carburized samples indicate that the MoC_y species remain bonded to framework oxygens. This is consistent with the findings that the total oxygen removed upon exposure to CH_4 at 973 K, determined by measuring the evolved CO_2, CO, and H_2O, corresponds to 2.5 oxygen atoms per Mo atom (36), and that carburization does not re-form the Brønsted acid sites as determined by measuring the intensity of OH stretching infrared band (27). These active centers appear to reside within ZSM5 channels and contain both Mo–O and Mo–C bonds, which may account for their greater resistance to carbon deposition than bulk Mo_2C during CH_4 pyrolysis reaction (46). Alternatively, the Mo–O bonds could simply serve as an anchor point for isolated Mo species, and the restricted ZSM5 channel geometry may instead be solely responsible for the observed inhibition of carbon deposits during CH_4 reactions.

TABLE 3

Refined Structural Parameters Describing Mo Structure in Carburized Catalyst

Shell	Coordination number	Interatomic distance (Å)	E_0 shift (eV)	Relative area under EXAFS paths
Mo–C	3.2 ± 0.011	2.090 ± 0.00055	1.7 ± 0.025	100%
Mo–O	0.9 ± 0.0046	1.705 ± 0.00066	-4.2 ± 0	52.45%
Mo–Al	2.1 ± 0.026	3.656 ± 0.0013	-3.0 ± 0	21.46%
Mo–Mo	0.1 ± 0.0070	2.795 ± 0.0028	0	3.98%

Note. Debye-Waller factors were fixed at zero and the value of S_0^2 was 0.70.

4. CONCLUSIONS

The *in situ* Raman and X-ray absorption results reported here confirmed the $(Mo_2O_5)^{2+}$ dimer structure proposed earlier from the stoichiometry of the solid-state exchange processes (1). Raman spectra of the exchanged samples

showed that MoO_3 spread and migrated into the ZSM5 channel to form dispersed MoO_x species. These results are consistent with the proposed mechanism for solid-state migration of MoO_3 on H-ZSM5 (1). Above 623 K, MoO_x migrates as $(MoO_3)_n$ oligomers on the external surface of H-ZSM5. Between 773 and 973 K, MoO_x species enter ZSM5 channels, exchange with acid sites, and acquire tetrahedral symmetry. The Mo K-edge spectra of exchanged samples resemble that of $MgMo_2O_7$, suggesting that the local structure of MoO_x species in the exchanged sample is similar to the ditetrahedral structure of the isolated dimolybdate species in $MgMo_2O_7$. Cluster simulations of the radial structure function of the exchanged MoO_x species are consistent with $(Mo_2O_5)^{2+}$ cations bridging two Al sites and connected to two zeolite framework oxygens. These ditetrahedral species reduce and carburize to form dispersed MoC_y species in CH_4 at 973 K. the resulting structures retain a Mo bond to a framework oxygen. Raman spectra show that after 9 h at 973 K, some MoO_x remains as isolated MoO_x species on the external ZSM5 surface. These species convert to Mo_2C in CH_4 at 973 K, but they are a relatively minor species compared to the exchanged MoC_y species and they are likely to deactivate rapidly during CH_4 pyrolysis reactions at 973 K in the unprotected environment of external zeolite surfaces.

ACKNOWLEDGMENTS

The authors thank Dr. Young-Ho Kim for measuring the initial CH_4 conversion reactivity results as shown in Fig. 9, and Mr. Bryan Olthof for his help with the Raman set-up. X-ray absorption data were collected at the Stanford Synchrotron Radiation Laboratory (SSRL), which is operated by the Department of Energy (DOE), Office of Basic Energy Sciences under Contract DE-ACO3-76SF00515. Richard Borry was supported by a National Science Foundation Fellowship. Project funding was provided by the Federal Energy Technology Center (U.S. Department of Energy, Contract DE-AC03-76SF00098) under the technical supervision of Dr. Daniel Driscoll.

REFERENCES

1. Borry, R. W., Kim, Y.-H., Huffsmith, A., Reimer, J. A., and Iglesia, E., *J. Phys. Chem.* **103**, 5787 (1999).
2. Wang, L., Tao, L., Xie, M., and Xu, G., *Catal. Lett.* **21**, 35 (1993).
3. Solymosi, F., Erdohelyi, A., and Szoke, A., *Catal. Lett.* **32**, 43 (1995).
4. Wang, D., Lunsford, J. H., and Rosynek, M. P., *Topics Catal.* **3**, 289 (1996).
5. Liu, S., Dong, Q., Ohnishi, R., and Ichikawa, M., *J. Chem. Soc. Chem. Commun.*, 1455 (1997).
6. Mestl, G., and Srinivasan, T. K. K., *Catal. Rev.* **40**, 451 (1998).
7. Jeziorowski, H., and Knozinger, H., *J. Phys. Chem.* **83**, 1166 (1979).
8. Kim, D. S., Wachs, I. E., and Segawa, K., *J. Catal.* **146**, 268 (1994).
9. Knozinger, H., and Taglauer, E., "Catalysis Specialist Periodical Report." Royal Soc. Chem., London, 1993.
10. Hardcastle, F. D., and Wachs, I. E., *J. Raman Spectrosc.* **21**, 683 (1990).
11. Meitzner, G., *Catal. Today* **39**, 281 (1998).
12. Sayers, D. E., Lytle, F. W., and Stern, E. A., *Phys. Rev. Lett.* **27**, 1204 (1971).
13. Imamura, S., Sasaki, H., Shono, M., and Kanai, H., *J. Catal.* **177**, 1 (1998).
14. Miyanaga, T., Matsubayashi, N., Fukumoto, T., Yokoi, K., Watanabe, I., Murata, K., and Ikeda, S., *Chem. Lett.*, 487 (1988).
15. Aritani, H., Tanaka, T., Funabiki, T., Yoshida, S., Kudo, M., and Hasegawa, S., *J. Phys. Chem.* **100**, 5440 (1996).
16. Cramer, S. P., Eccles, T. K., Kutzler, F. W., Hodgson, K. O., and Mortenson, L. E., *J. Am. Chem. Soc.* **98**, 1287 (1976).
17. Djajanti, S. D., and Howe, R. F., *Stud. Surf. Sci. Catal.* **105C**, 2067 (1997).
18. Olthof, B., Master's thesis, University of California, Berkeley, 1998.
19. Bearden, J. A., and Burr, A. F., *Rev. Mod. Phys.* **29**, 125 (1967).
20. Stadnicka, K., Haber, J., and Kozlowski, R., *Acta Crystallogr* **B33**, 3859 (1977).
21. Lee, J. S., Oyama, S. T., and Boudart, M., *J. Catal.* **125**, 157 (1990).
22. Barton, D. G., Ph.D. dissertation, University of California, Berkeley, 1998.
23. Ressler, T., *WinXAS 97*, version 1.2, 1998.
24. Zabinsky, S. I., Rehr, J. J., Ankudinov, A., Albers, R. C., and Eller, M. J., *Phys. Rev. B* **52**, 2995 (1995).
25. Li, C., and Stair, P. C., *Catal. Today* **33**, 353 (1997).
26. Deleted in proof.
27. Li, W., Meitzner, G. D., Kim, Y.-H., Borry, R. W., and Iglesia, E., submitted for publication.
28. Huang, Y., *J. Am. Chem. Soc.* **118**, 7233 (1996).
29. Dutta, P. K., Rao, K. M., and Park, J. Y., *J. Phys. Chem.* **95**, 6654 (1991).
30. Leyrer, J., Mey, D., and Knozinger, H., *J. Catal.* **124**, 349 (1990).
31. Brown, R. G., and Ross, S. D., *Spectrochim. Acta* **28A**, 1263 (1972).
32. Deo, G., and Wachs, I. E., *J. Phys. Chem.* **95**, 5889 (1991).
33. Chen, L., Lin, L., Xu, Z., Li, X., and Zhang, T., *J. Catal.* **157**, 190 (1995).
34. Mestl, G., and Knözinger, H., *Langmuir* **14**, 3964 (1998).
35. Shadle, E., Hedman, B., Hodgson, K. O., and Solomon, E. I., *Inorg. Chem.* **33**, 4235 (1994).
36. Kim, Y.-H., Borry, R. W., and Iglesia, E., *Microporous Mater.*, in press.
37. Schuurman, Y., Decamp, T., Pantazidis, A., Xu, Y.-D., and Mirodatos, C., *Stud. Surf. Sci. Catal.* **109**, 351 (1997).
38. Seleborg, M., *Acta Chem. Scand.* **21**, 499 (1967).
39. Xu, Y., Shu, Y., Liu, S., Huang, J., and Guo, X., *Catal. Lett.* **35**, 233 (1995).
40. Zhang, J.-Z., Long, M. A., and Howe, R. F., *Catal. Today* **44**, 293 (1998).
41. "The Tables of Interatomic Distances and Configuration in Molecules and Ions." Chemical Society Special Publication No. 11, London, 1958.
42. Lee, J. S., Oyama, S. T., and Boudart, M., *J. Catal.* **106**, 125 (1987).
43. Solymosi, F., Cserenyi, J., Szoke, A., Bansagi, T., and Oszko, A., *J. Catal.* **165**, 150 (1997).
44. Wang, D., Lunsford, J. H., and Rosynek, M. P., *J. Catal.* **169**, 347 (1997).
45. Liu, S., Wang, L., Ohnishi, R., and Ichikawa, M., *J. Catal.* **181**, 175 (1997).
46. Solymosi, F., Szoke, A., and Cserenyi, J., *Catal. Lett.* **39**, 157 (1996).